Resonance Raman scattering in InSb: Deformation potentials and interference effects at the E_1 gap

J. Menéndez, L. Viña,* M. Cardona, and E. Anastassakis†
Max-Planck-Institut für Festkörperforschung, Heisenbergstrasse 1, D-7000 Stuttgart 80, Federal Republic of Germany
(Received 15 March 1985)

This paper presents a reevaluation of the optical-phonon deformation potential constants near the E_1 gap of InSb. The absolute values of the deformation potentials $d^5_{1,0}$ and $d^5_{3,0}$ are obtained from a measurement of the Raman efficiency for allowed LO-phonon scattering and a fit of previous uniaxial-stress experiments by using new ellipsometric data for the optical susceptibility. The signs of the deformation potentials are deduced from a study of the interference between the amplitudes for forbidden and allowed LO-Raman scattering. The values obtained are $d^5_{1,0}=-16.2\pm4$ eV and $d^5_{3,0}=32.9\pm8$ eV. The study of the interference also provides information about the relative weight of different sources of forbidden LO-Raman scattering.

I. INTRODUCTION

The existence of resonance in the efficiency for Raman scattering by phonons near the E_1 edge of InSb was first suggested by Pinczuk and Burstein.[1] This effect was confirmed by Leite and Scott for InAs.[2] The detailed investigation of these phenomena, however, had to await the advent of the cw dye laser.[3,4] Measurements of E_1 resonances were performed for Ge and InSb (Refs. 3–7) since these resonances occur in the lasing range of the Rhodamine-6G dye, one of the most efficient dyes for cw operation and the first one used.

The detailed study of the resonance behavior of the Raman efficiency near electronic critical points provides information about the electron-phonon interaction. In covalent semiconductors such as Si and Ge, this interaction is of short range[8] and characterized by the so-called "deformation potentials" (DP's).[8–10] The longitudinal-optical (LO) phonons in polar semiconductors such as InSb produce a macroscopic electric field, which interacts with the electrons. This coupling, of long range, is known as the Fröhlich interaction. The Fröhlich interaction is responsible for the dipole-forbidden LO-Raman scattering observed for laser energies near critical points. The coupling constant, normally written as C_F,[9,10] can be expressed in terms of the static and high-frequency dielectric constants. The coupling parameters of the DP interaction are of more interest, because they are related to the details of the electronic band structure of the material under consideration. The deformation potentials can be obtained from measurements of the absolute Raman efficiencies. However, their sign remains undetermined, unless some other scattering mechanism interferes with the amplitude for DP-induced Raman scattering.[10]

In this paper we present a reevaluation of the DP constants $d^5_{1,0}$ and $d^5_{3,0}$ (Kane's notation[9,10]) for the E_1 gap and its spin-orbit partner $E_1+\Delta_1$ along the [111] direction in the Brillouin zone of the InSb. We also perform the first experimental determination of their sign. To that purpose we study the interference between the amplitudes for allowed (DP-induced) and forbidden (Fröhlich-induced) LO-Raman scattering.[11] This study also provides information about the relative contribution of different possible sources of forbidden LO-Raman scattering.

Within the scope of the adiabatic approximation (the limit in which the phonon frequency tends to zero), the components of the Raman tensor for DP-induced scattering can be written in terms of the optical susceptibility and its first derivative. Two possible procedures can be adopted in order to evaluate the Raman tensor: One can use either experimental optical data or approximate analytical expressions for the optical susceptibility obtained from a model description of the critical points. The latter procedure has been often used near the E_0 and $E_0+\Delta_0$ transitions at the Γ point.[9,10] On the other hand, previous investigators have analyzed their Raman data near the E_1 gap in terms of experimental values of the optical susceptibility, in the hope of including excitonic effects which are difficult to treat in analytic form.[3,5–7] This method, however, has the shortcoming that one needs a complicated numerical manipulation of the optical data to separate the contributions of the E_1 and $E_1+\Delta_1$ gaps. On the other hand, the main effect of the excitonic interaction on the susceptibilities can be represented[12,13] by a multiplicative factor of the form $Ae^{i\psi}$. This factor mixes real and imaginary parts of the susceptibility, but only multiplies by A^2 the Raman efficiency, which is proportional to the square of the magnitude of the Raman tensor. Hence, introducing the excitonic interaction should only enhance the calculated Raman efficiency, but not change its functional dependence on the laser frequency.

We thus adopt the following procedure to evaluate the Raman tensor.[14] We describe the E_1 and $E_1+\Delta_1$ gaps as two-dimensional interband minima and then fit the standard expression for the susceptibility at these critical points to our experimental data for the optical constants, whereby the analytic expressions are multiplied by factors $Ae^{i\psi}$ and a broadening parameter is introduced. The resulting expressions are used to evaluate the Raman tensor.

With the Raman tensor so calculated we attempt to fit previous resonant experiments under uniaxial stress[7] and to calculate the interference effects between allowed and forbidden LO-Raman scattering, using published analytic expressions for the forbidden contribution.

The fits we obtain to previous resonance experiments under uniaxial stress[7] for transverse-optical (TO)—phonon Raman scattering are of similar quality as those obtained in Ref. 7, but the corresponding deformation potentials are in much better agreement with the theoretical predictions. The analysis of the inteference experiments confirms the theoretically predicted signs of the deformation potentials involved. On the other hand, this analysis suggests that impurities produce the most important scattering mechanism for forbidden LO-Raman scattering, as proposed by Gogolin and Rashba.[15]

II. EXPERIMENTAL

Our sample was a (001)-oriented slab of undoped InSb. At 100 K, the sample is p type with $R_H=230$ cm^3/C and $\rho=0.8$ Ω cm.[16] The optical susceptibility was measured by ellipsometry as described elsewhere.[12,13] We used for both ellipsometry and Raman scattering the surface treatment described in Ref. 13.

Our coordinate system is x ([100]), y ([010]), z ([001]), x' ([110]), y' ([1$\bar{1}$0]). In the scattering configuration $z(x,y)\bar{z}$ [the coordinates inside (outside) the brackets indicate the polarization (wave vector) of the light], Raman scattering by LO phonons is dipole allowed. The dipole selection rules forbid Raman scattering by LO phonons in the $z(x,x)\bar{z}$ and $x(y,y)\bar{z}$ configurations.[9,10] However, the LO peak can be observed in these configurations for laser energies near critical points. This violation of the dipole selection rules is due to the q-dependent contribution of the Fröhlich interaction.[9,10] Both allowed and "forbidden" Raman scattering by LO phonons are present in the $z(x',x')\bar{z}$ and $z(y',y')\bar{z}$ configurations. Thus one expects for these configurations to observe interferences between the amplitudes for forbidden and allowed scattering.

We cut three thin rectangular slabs with the long sides parallel to [100], [110], and [1$\bar{1}$0]. The three samples were glued to the cold finger of a N_2 cryostat with the long sides in vertical position. A Si slab was added in order to determine scattering rates by the sample substitution method.[10] A simple horizontal shift of the Dewar was needed to change the scattering configuration. The [110] and [1$\bar{1}$0] directions were identified by chemical etching.[11] [The sample was immersed at room temperature for one minute in a solution of one part FH (48%) and three parts H_2O_2 (15%) after finishing the Raman measurements and the etch pattern observed with a microscope.]

The measurements were performed with a dye laser, using Rhodamine-6G pumped with a cw Ar^+ laser. The light beam was focused onto the sample with a cylindrical lens. The scattered light was analyzed with a 1-m—Jarrell-Ash double monochromator and detected by photon counting.

The Stokes scattering rate outside the sample can be written

$$R_S'=\left\{\frac{T_S T_L P_L' \omega_S^3[n(\Omega_{\rm ph})+1]}{(\alpha_L+\alpha_S)n_S n_L M^* \Omega_{\rm ph} v_c}\right\}\frac{\Delta\Omega'}{2c^4}\,|\hat{\mathbf{e}}_S\cdot\overleftrightarrow{R}\cdot\hat{\mathbf{e}}_L|^2\,, \quad (1)$$

where P_L' is the incident laser power; $T_{S,L}=1-r_{S,L}$, where r is the power reflectivity and the subscript L (S) means that it is evaluated at the incident (scattered) frequency; α the absorption coefficient; n the refractive index; ω_S the scattered frequency; M^* the reduced mass of the primitive cell; v_c the volume of the primitive cell; $\Omega_{\rm ph}$ the Raman phonon frequency; $n(\Omega_{\rm ph})$ the phonon occupation factor; c the speed of light in vacuum; and $\Delta\Omega'$ the solid angle of collection *outside* the crystal. The last factor defines the Raman tensor $\overleftrightarrow{R}$ which is contracted with the light polarization vectors $\hat{\mathbf{e}}_L$ and $\hat{\mathbf{e}}_S$. The independent components of $\overleftrightarrow{R}$ are called Raman polarizabilities.[10] In the dipole approximation, symmetry allows only one such component for diamond- and zinc-blende semiconductors, usually called α.[10]

Equation (1) can be used to obtain absolute values of the Raman polarizability by the sample substitution method, measuring simultaneously a sample of known α. We use silicon as a reference. Its Raman polarizability is known[17] although the error margin is large (we take, at $\omega_L=2.0$ eV, $|\alpha|=40\pm10$ Å^2). The expression in the curly brackets of Eq. (1) takes different values for Si and InSb and has to be evaluated for each material. The optical constants required for InSb were obtained from our ellipsometric data. For Si, we used absorption data from Dash and Newman[18] and additional data from Aspnes and Studna.[19]

III. RESULTS

A. Ellipsometric data

We have reevaluated the optical constants of InSb by using a digital rotating analyzer ellipsometer. Our results for the optical susceptibility χ ($\epsilon=1+4\pi\chi$) and its derivative $d\chi/dE$ are shown in Fig. 1. Also shown are the results of Shaklee *et al.* for $d\chi/dE$ obtained with wavelength modulation spectroscopy.[20] The most important difference between the two sets of data is the minimum of Im($d\chi/dE$), which in Ref. 20 is strongly enhanced. Due to the very large longitudinal mass in the [111] direction, the E_1 and $E_1+\Delta_1$ gaps of InSb can be considered to correspond to a $2d$ interband minimum. The optical susceptibility associated with these transitions is

$$\chi(E)=\chi^+(E)+\chi^-(E)\,, \quad (2)$$

where χ^+ is the contribution of the E_1 gap and χ^- the contribution of the $E_1+\Delta_1$ gap. The functions $\chi^\pm$ are approximately given by[10]

$$\chi^+(E)=-\frac{A^+}{E^2}(E_1+\Delta_1/3)\ln[1-(E/E_1)^2]\,, \quad (3a)$$

$$\chi^-(E)=-\frac{A^-}{E^2}(E_1+2\Delta_1/3)\times\ln\{1-[E/(E_1+\Delta_1)]^2\}\,. \quad (3b)$$

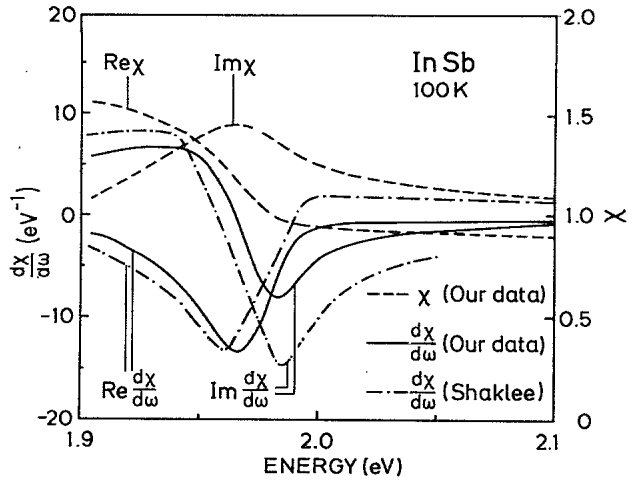

FIG. 1. Optical susceptibility of InSb. The solid and dashed lines represent our ellipsometric measurements. The dot-dashed line indicates the wavelength modulation data of Ref. 8.

Theory predicts $A^+ \simeq A^- \simeq 4\sqrt{3}e^2/9\pi a_0 = 0.54$ eV. Here e is the free-electron charge and a_0 the lattice constant.

The experimental data of Fig. 1 were fitted with Eqs. (2) and (3) taking A^+, A^- as adjustable parameters; adding a small imaginary part to the gaps, $E_1 \rightarrow E_1 - i\eta^+$, $E_1 + \Delta_1 \rightarrow E_1 + \Delta_1 - i\eta^-$; and multiplying χ^+ and χ^- by factors $e^{i\psi^\pm}$, to take into account excitonic effects.[12,13] In order to eliminate the weakly dispersive contribution of lower and higher interband transitions, the fits are performed to the second energy derivative of χ. The fitted parameters are $A^+ = 0.54$ eV, $A^- = 0.44$ eV, $E_1 = 1.972$ eV, $\Delta_1 = 0.498$ eV, $\eta^+ = 0.022$ eV, $\eta^- = 0.027$ eV, and $\psi^+ \sim \psi^- \simeq \pi/2$. These values of ψ^+, ψ^- mean that the excitonic effects are so strong that the critical point can be described as a $2d$ saddle point instead of a $2d$ minimum. Whereas fits of this type give an excellent agreement with our ellipsometric data, they deviate considerably from those of Shaklee *et al.*[20] We have also performed room-temperature measurements and found an excellent agreement with earlier ellipsometric data.[19,21] We therefore believe our results at 100 K to be more reliable than those of Ref. 20.

The function $\chi(E)$ was determined in Ref. 5 by integrating Shaklee's[20] $d\chi/dE$. The values found for the imaginary part of χ (Fig. 2 of Ref. 5) seem to be too large as compared with the present ones. The real part is shifted due to the arbitrary integration constant. The jump at E_1 is again too large compared with our experimental χ.

B. Raman experiment

Our Raman results are shown in Fig. 2(a). Contrary to the case of the $E_0 + \Delta_0$ resonance in GaAs,[11] the *two* configurations where we expect interferences show strong maxima at the position where the strongest interference would be expected.

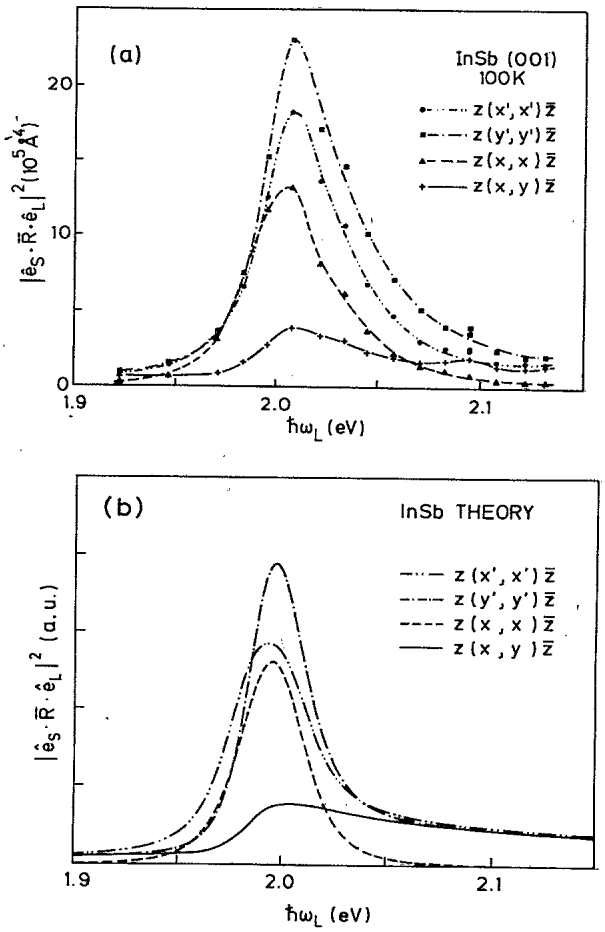

FIG. 2. (a) Resonant Raman scattering (RRS) spectra of LO phonons near the E_1 gap of InSb. The tensor components measured in each configuration are indicated in Eq. (14). (b) Calculated RRS spectra of LO phonons. See Sec. IV C.

IV. THEORY

A. Raman scattering by TO phonons

Transverse-optical phonons produce Raman scattering only via the DP interaction. The Raman polarizability near the E_1 gap is given by[10]

$$a = \frac{a_0^2}{4\sqrt{6}} \left[-\frac{1}{2\sqrt{2}} d_{1,0}^5 \frac{d\chi(E)}{dE_1} + 2d_{3,0}^5 \frac{\chi^+(E) - \chi^-(E)}{\Delta_1} + C \right]. \quad (4)$$

The constant C represents the contribution of interband transitions far from the E_1 and $E_1 + \Delta_1$ gaps. The first term in the large parentheses arises from two-band processes produced by the phonon modulation of the gap. They are characterized by the deformation potential $d_{1,0}^5$. The coupling of the two spin orbit-split valence bands by the phonon produces the second term in Eq. (4). The strength of this coupling is measured by the deformation potential $d_{3,0}^5$. Equation (2) has been derived within the

adiabatic approximation ($\omega_L \simeq \omega_S$). If the phonon energy $\hbar\Omega_{\rm ph}$ is not negligible with respect to $|\hbar\omega_L - E_1 + i\eta|$, the derivative in Eq. (4) must be replaced by a finite difference of the susceptibility evaluated at $E=\hbar\omega_L$ and $\hbar\omega_S$. However, we have checked that for $\hbar\Omega_{\rm ph} \sim \eta^{\pm}$, as in our case, the error introduced by the adiabatic approximation is less than 5% if the gap is renormalized to $E_1 \rightarrow E_1 + \hbar\Omega_{\rm ph}/2$. The two-band terms, which are proportional to the derivative of the susceptibility, produce a sharp resonance at the E_1 gap, while the three-band terms, proportional to the susceptibility itself, give rise to a broader resonance extending from E_1 to $E_1+\Delta_1$. The relative weight of the two contributions depends on the values of the deformation potentials $d^5_{1,0}, d^5_{3,0}$ and on the spin-orbit parameter Δ_1. Whereas the deformation potentials have roughly the same values for III–V and group IV semiconductors, the spin-orbit splitting is much larger for materials with high atomic number. For example, the spin-orbit splitting is $\Delta_1 = 0.187$ eV in Ge and 0.498 eV for InSb.[12,13] We then expect a relatively stronger two-band contribution in InSb, because the parameter Δ_1 appears in the denominator of the second term in Eq. (4). This fact can be confirmed by comparing the shape of both resonances. The relative importance of two- and three-band contributions also manifests itself in Raman experiments under uniaxial stress.

For uniaxial stress along the [111] direction, the E_1 gap splits into a singlet and a triplet,[7,9,10] and the Raman tensor now has two independent components. For the scattering configuration $\hat{\mathbf{e}}_S || \hat{\mathbf{e}}_L ||$ [111], the tensor component has the form[7,9,10]

$$A = \frac{a_0^2}{12\sqrt{2}} \left[-\frac{1}{2\sqrt{2}} d^5_{1,0} \frac{9}{4} \left[\frac{d\chi^S}{dE_1} - \frac{5}{9} \frac{d\chi^T}{dE_1} \right] + 2 d^5_{3,0} \left[\frac{\chi^+ - \chi^-}{\Delta_1} \right]^T + C \right], \tag{5}$$

where the superscripts S and T mean that the functions are evaluated at the position of the singlet (S) or triplet (T) gap under stress.

Equation (5) shows that the scattering rate can be enhanced up to a factor $(\frac{9}{4})^2 \approx 4$ by applying stress in the [111] direction. The actual enhancement depends on the shift of the gaps under stress and on the relative magnitude of $d^5_{1,0}$ and $d^5_{3,0}$. Notice that the enhancement *only* arises from the two-band terms. Experimental results for Ge and InSb (Ref. 7) give $d^5_{3,0}/d^5_{1,0} = -7$ (InSb) and $d^5_{3,0}/d^5_{1,0} = -1.5$ (Ge). Nonlocal pseudopotential calculations[22,10] yield $d^5_{3,0}/d^5_{1,0} = -2.1$ for InSb and $d^5_{3,0}/d^5_{1,0} = -2.8$ for Ge at the L point of the Brillouin zone. The individual deformation potentials (Refs. 22 and 10) are $d^5_{1,0} = -18.2$ eV (InSb) and $d^5_{1,0} = -17.2$ eV (Ge). The signs are chosen such that a positive $d^5_{1,0}$ means that the E_1 gap along [111] increases for a [111] polarized phonon amplitude which increases the length of the bond along the [111] direction. The discrepancies between theoretical estimates and experimental values of the deformation potentials are discussed below.

B. Allowed Raman scattering by LO phonons

For LO phonons, the electron-phonon interaction can be written as a sum of the deformation-potential contribution plus the Fröhlich Hamiltonian, which arises from the macroscopic electric field generated by LO vibrations.

The *interband* terms of the Fröhlich Hamiltonian (electro-optic interaction) give an additional contribution to the Raman tensor,[10] which can be written for backscattering at the (001) face:

$$\overleftrightarrow{R} = \begin{bmatrix} 0 & a & 0 \\ a & 0 & 0 \\ 0 & 0 & 0 \end{bmatrix}, \tag{6}$$

where now a is a sum of a deformation-potential part like Eq. (4) plus an electro-optical contribution. Notice that the electro-optical and deformation-potential interactions generate Raman tensor contributions of the same symmetry.

The electro-optic contribution has been shown to be small in InSb (Ref. 6) and will not be taken into account in fitting the interferences. In other words, the Raman polarizability associated with allowed LO scattering will be taken from Eq. (4).

C. Forbidden LO-Raman scattering

Near critical points LO scattering is found for configurations with $\hat{\mathbf{e}}_L || \hat{\mathbf{e}}_S$ which are forbidden, according to the tensor in Eq. (6). The results can be explained by assuming that there is an additional diagonal contribution to the Raman tensor:

$$\overleftrightarrow{R}_F = \begin{bmatrix} a_F & 0 & 0 \\ 0 & a_F & 0 \\ 0 & 0 & a_F \end{bmatrix}. \tag{7}$$

This is the so-called forbidden LO scattering. [The word forbidden means that the dipole selection rules from Eq. (6) are violated. However, near resonance the scattered intensity is often stronger for forbidden than for allowed scattering.] There are different sources of forbidden LO scattering. First, the fact that the Raman phonon wave vector is not exactly zero leads to a contribution of the *intraband* terms of the Fröhlich interaction. For this process, the diagonal contribution near the E_1 gap can be written[7]

$$a_F = iq \frac{\sqrt{3}}{4\pi} \left[\frac{e}{m} \right]^2 \frac{1}{\omega_L} \left[\frac{1}{\omega_L \omega_S} \right]^{1/2} C_F (s_e - s_h) \times P^2 \left[\frac{2M^* \Omega_{\rm LO} v_c}{\hbar} \right]^{1/2} \frac{1}{a^*} \frac{1}{(\hbar\Omega_{\rm LO})^2} \times \left[2 - (\alpha+\beta) \ln \frac{\alpha}{\beta} \right], \tag{8a}$$

$$\alpha = \frac{\hbar\omega_L + i\eta - E_1}{\hbar\Omega_{\rm LO}}, \quad \beta = \alpha - 1, \tag{8b}$$

where e and m are the free-electron charge and mass; C_F is the Fröhlich constant $C_F=[2\pi e^2(1/\epsilon_\infty - 1/\epsilon_0)\hbar\Omega_{\rm LO}]^{1/2}$; $\Omega_{\rm LO}$ the LO-phonon frequency; P the momentum matrix element $1/i<x\,|\,p_x\,|\,s>=P$; $s_{e,h}=m_{\perp e,h}/(m_{\perp e}+m_{\perp h})$, with $m_{\perp e}$ ($m_{\perp h}$) being the transverse effective electron (hole) mass; and $a^*=(\hbar/2\mu_\perp\Omega_{\rm LO})^{1/2}$, where $\mu_\perp$ is the transverse reduced mass.

An additional, surface-field-induced forbidden LO scattering has been proposed by Pinczuk and Burstein.[1] This effect can be treated in fourth-order perturbation theory. The result for backscattering at the (001) face is[7]

$$a_F=iq\frac{\sqrt{3}}{4\pi}\left[\frac{e}{m}\right]^2\frac{1}{\omega_L}\left[\frac{1}{\omega_L\omega_S}\right]^{1/2}C_F(s_e-s_h)\times P^2\left[\frac{2M^*\Omega_{\rm LO}v_c}{\hbar}\right]^{1/2}\frac{1}{a^*}\frac{1}{(\hbar\Omega_{\rm LO})^3}\times\frac{\partial}{\partial\alpha}\left[2-(\alpha+\beta)\ln\left[\frac{\alpha}{\beta}\right]\right]. \tag{9}$$

The feature common to intraband-Fröhlich [Eq. (8)] and electric-field-induced scattering [Eq. (9)] is that the phonon created in the scattering process has a wave vector given by $\mathbf{q}=\mathbf{k}_L-\mathbf{k}_S$, exactly like in the allowed case. Hence, if we choose a configuration where both effects occur, they might interfere because the final states are the same. Scattering by impurities as a source of forbidden scattering has been proposed by Gogolin and Rashba and was recently shown to be important in GaAs (Ref. 11) and CdTe.[23] This process is also of fourth order in perturbation theory. The virtual electron-hole pair created by the light is successively scattered by the Fröhlich interaction and by an impurity before recombining. The important difference with the two previous mechanisms is that instead of a phonon with $\mathbf{q}=\mathbf{k}_L-\mathbf{k}_S$, a distribution of phonons is created, having mostly a larger wave vector. A calculation of this process for a three-dimensional critical point was presented in Ref. 11. Although no theoretical evaluation is available for the E_1 gap, we can anticipate some characteristics: Because the phonon wave vector is not fixed by the rule $\mathbf{q}=\mathbf{k}_L-\mathbf{k}_S$, the scattering mechanism will select mainly those q vectors which produce the simultaneous cancellation of two denominators in the perturbative expansion of the Raman polarizability. This effect is called "double resonance."[24] The condition can be achieved for $\hbar\omega_S\approx E_1$, leading to a strong outgoing resonance, i.e., the maximum of the forbidden resonance for this process tends to occur at $\hbar\omega_L=E_1+\hbar\Omega_{\rm LO}$. This is $\frac{1}{2}\hbar\Omega_{\rm LO}$ higher than the resonances from Eqs. (8) and (9), which have maxima at $\hbar\omega_L=E_1+\frac{1}{2}\hbar\Omega_{\rm LO}$.

The impurity-induced Raman tensor has the form

$$\overleftrightarrow{R}_{Fi}=\begin{bmatrix}a_{Fi}&0&0\\0&a_{Fi}&0\\0&0&a_{Fi}\end{bmatrix}. \tag{10}$$

Possible off-diagonal matrix elements are expected to be very small.[7]

D. Interference effects

As discussed above in allowed LO scattering, the same final state is reached as in forbidden LO scattering due to the intraband-Fröhlich or the electric-field mechanism. Hence for backscattering at the (001) face we have to add the Raman tensors. We thus obtain a total Raman tensor given by

$$\overleftrightarrow{R}=\begin{bmatrix}a_F&a&0\\a&a_F&0\\0&0&a_F\end{bmatrix}, \tag{11}$$

where a_F is obtained by adding Eqs. (8) and (9). This tensor has to be used in Eq. (1). On the other hand, since impurity-induced forbidden scattering produces different final states, the corresponding tensor [Eq. (10)] has to be squared and added to the square of Eq. (11). The final result for the configurations we want to measure is

$$R_S'\propto\begin{cases}|a_F+a|^2+|a_{Fi}|^2 & \text{for } z(x',x')\bar{z}\\ |a_F-a|^2+|a_{Fi}|^2 & \text{for } z(y',y')\bar{z}\\ |a_F|^2+|a_{Fi}|^2 & \text{for } z(x,x)\bar{z}\\ |a|^2 & \text{for } z(x,y)\bar{z}\,.\end{cases} \tag{12}$$

Hence, if the impurity mechanism dominates, the configurations $z(x',x')\bar{z}$ and $z(y',y')\bar{z}$ should give the same result, whereas we expect a different behavior if the other two mechanisms play an important role.

In Sec. VI we shall attempt to explain the curves of Fig. 2(a) using an expression similar to Eq. (12) together with Eqs. (4) and (8).

V. REEVALUATION OF THE UNIAXIAL-STRESS EXPERIMENTS

In view of the differences between our ellipsometric data and the results of Shaklee *et al.* for the optical susceptibility,[20] we want to recalculate the resonance of the TO-Raman scattering under uniaxial stress measured in Ref. 7 and shown here in Fig. 3(a). We use Eq. (5) together with Eqs. (3a) and (3b) and the parameters for the optical susceptibility determined in Sec. III. The prefactors $e^{i\psi^\pm}$ are dropped: They should not affect the Raman result if, as is true in our case, $\psi^+\approx\psi^-$. The constant C in Eq. (5) is set equal to zero. This is consistent with the fact that the Raman efficiency is very small below E_1 and above $E_1+\Delta_1$,[5,6] thus indicating that contributions from other interband transitions can be neglected in this energy range. The results are shown in Fig. 3(b). The increase in the strength of the resonance with increasing stress found experimentally is well reproduced by the calculations. The calculated shift of the peak energy with increasing stress, however, is about a factor of 2 smaller than observed experimentally. The deformation-potential ratio $d^5_{3,0}/d^5_{1,0}=-2.0$ which gives the best agreement between theory and experiment agrees also with theoretical estimates at the L point.[10,22]

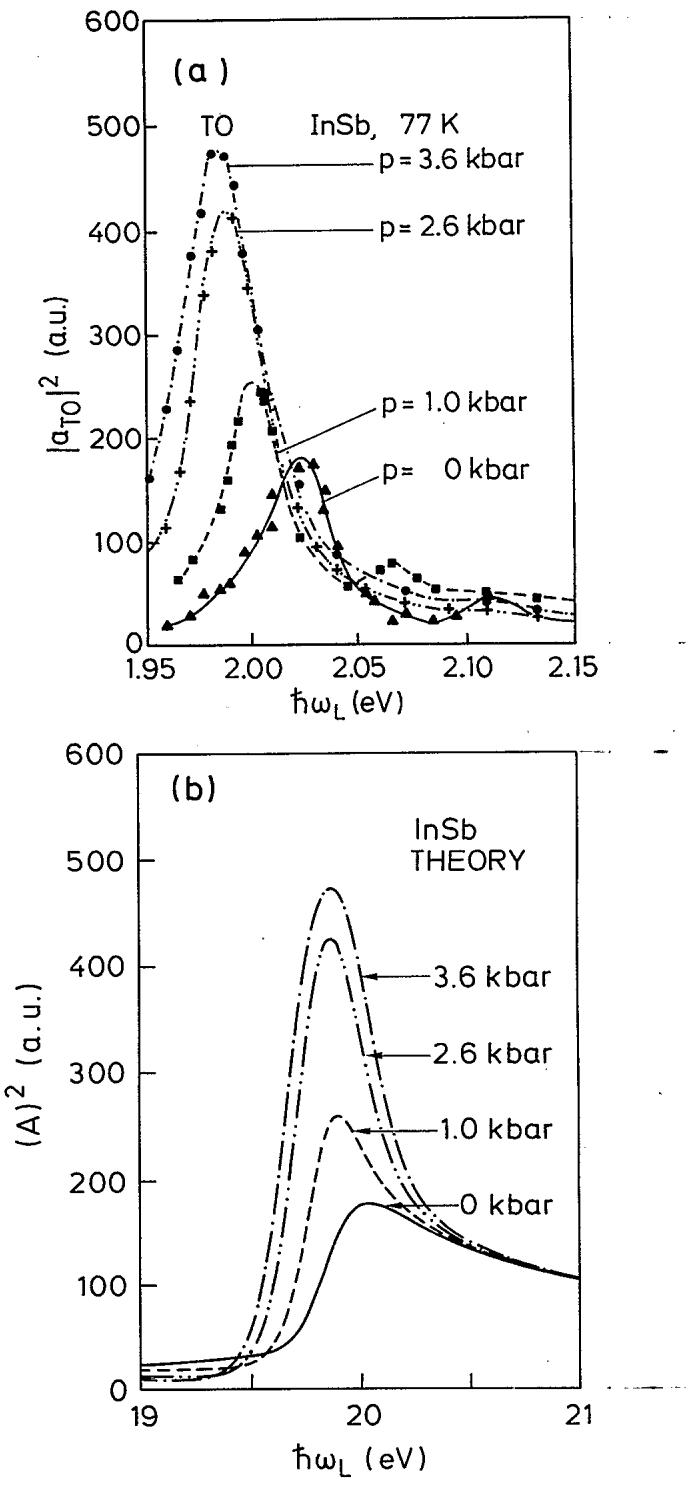

FIG. 3. RRS spectra of TO phonons in InSb near E_1. (a) Experimental results [Fig. 2(a), Ref. 7]. (b) Calculated curves with our ellipsometric data for the optical susceptibility.

VI. INTERFERENCE EFFECTS BETWEEN ALLOWED AND FORBIDDEN LO SCATTERING

Having determined the parameters for TO scattering, we now try to reproduce theoretically the experimental interference effects at the E_1 resonance shown in Fig. 2(a). We represent allowed LO scattering with Eq. (4), thus neglecting the electro-optic contribution as mentioned in Sec. III. For forbidden scattering, we have discussed in Sec. III three possible mechanisms. For the "interfering" part in Eq. (12) there are contributions from intraband-Fröhlich-induced and electric-field-induced processes as well. An attempt to distinguish between these two mechanisms in Ref. 7 failed because theory predicts for both not only a similar strength but also a similar dependence on uniaxial stress. In our fit we shall first assume that the intraband-Fröhlich mechanism is dominant and see whether we can represent the results of Fig. 2(a) with this assumption. Equation (8) for forbidden LO-Raman scattering has been deduced without including excitonic effects. Because it can be rewritten in terms of the second energy derivative of the susceptibility,[10] the effect of the excitonic interaction should also be represented by a factor of the form $e^{i\psi+}$. Thus the use of Eq. (8) is consistent with the dropping of such factors in the expression for the allowed Raman polarizability (Sec. V). Since no theoretical calculation of impurity-induced forbidden LO scattering near E_1 has been published, we have chosen to represent this contribution by a frequency-dependent tensor proportional to Eq. (8), but shifted $\hbar\Omega_{LO}/2$ to higher energies (see Sec. IV C). We introduce a parameter ε which represents the fraction of forbidden scattering which interferes coherently with the allowed one. The noninterfering fraction $1-\varepsilon$ corresponds presumably to impurity-induced scattering. In this sense we rewrite Eqs. (12) as[11]

$$|a'(\omega_L)+\varepsilon^{1/2}a'_F(\omega_L)|^2 + (1-\varepsilon)|a'_F(\omega_L-\Omega_{LO}/2)|^2 \quad \text{for } z(x',x')\bar{z}\,, \tag{13a}$$

$$|-a'(\omega_L)+\varepsilon^{1/2}a'_F(\omega_L)|^2 + (1-\varepsilon)|a'_F(\omega_L-\Omega_{LO}/2)|^2 \quad \text{for } z(y',y')\bar{z}\,, \tag{13b}$$

$$\varepsilon|a'_F(\omega_L)|^2+(1-\varepsilon)|a'_F(\omega_L-\Omega_{LO}/2)|^2 \quad \text{for } z(x,x)\bar{z}\,, \tag{13c}$$

$$|a'(\omega_L)|^2 \quad \text{for } z(x,y)\bar{z}\,. \tag{13d}$$

The primes over the a's mean that we represent them with the corresponding expressions Eqs. (4) and (8) times a multiplicative factor fitted to experiment. Following Eqs. (13a)–(13d), we first fit the configuration $z(x,y)\bar{z}$, using for $a'(\omega_L)$ an expression proportional to Eq. (4) with $d^5_{3,0}/d^5_{1,0}=-2.0$, and next the configurations $z(x,x)\bar{z}$, $z(x',x')\bar{z}$, and $z(y'y')\bar{z}$, using for a'_F a function proportional to Eq. (8a). We treat ε as an adjustable parameter. Figure 2(b) shows the results which reproduce best the experimental data of Fig. 2(a), found for $\varepsilon=0.05$. This small value of ε means that most of the forbidden scattering is impurity induced. This fit shows qualitative agreement with experiment, including the surprising result that both interference configurations have maxima at the postion where the strongest inteference is expected. This fact is directly related to the change of sign of $\mathrm{Im}(dX/dE)$ above E_1 which leads to a constructive interference for both configurations, in one case slightly above E_1, in the other slightly below. To obtain the

strongest constructive inteference for the configuration $z(y',y')\bar{z}$, one needs $d^5_{1,0}<0$ and $d^5_{3,0}>0$, in agreement with theoretical estimates.[10,22] Thus we have performed the first experimental determination of these signs.

The reasonable agreement between theory and experiment which is obtained by assuming that the interfering part of the forbidden tensor is due to the interband-Fröhlich mechanism, suggests that electric-field effects are not very important in this case: The additional frequency derivative in Eq. (9) should produce a very different interference resonance. A calculation of the forbidden polarizability with Eq. (8) yields $|\alpha_F|\approx 22$ Å^2, while the experimental value, assuming $\varepsilon=0.05$, is $|\alpha_F|\simeq 250$ Å^2. The discrepancy between theory and experiment is larger than that found previously for GaAs near $E_0+\Delta_0$,[11] but here the uncertainty is much larger, due to the much stronger impurity-induced scattering mechanism.

VII. DETERMINATION OF $d^5_{3,0}$ AND $d^5_{1,0}$

If we neglect the electro-optic contribution to allowed LO scattering, we can use our absolute measurements to determine the deformation potentials $d^5_{3,0}$ and $d^5_{1,0}$. We use Eq. (4) to fit our experimental results in the configuration $z(x,y)\bar{z}$ of Fig. 2(a). From the uniaxial-stress experiment we know that $d^5_{3,0}/d^5_{1,0}=-2.0$. From the interference experiment we know that $d^5_{3,0}>0$. Using these results we obtain $d^5_{1,0}=-16\pm4$ eV and $d^5_{3,0}=33\pm8$ eV. The error arises mainly from the uncertainty in the Raman polarizability of silicon.[17]

These deformation potentials should be compared with theoretical values found in the literature. In doing so, one must keep in mind that the experimental values represent an average of the values calculated at Λ points between $(\pi/a_0)(111)$ (the L point) and $(\pi/4a_0)(111)$. In Ref. 22 the value $d^5_{3,0}=38$ eV was calculated for InSb at the L point. A recent pseudopotential calculation[25] yields $d^5_{1,0}=-14$ eV and $d^5_{3,0}=32$ eV at the L point, while the Λ averages corresponding to the E_1 transitions are $d^5_{1,0}\approx-12$ eV and $d^5_{3,0}\approx 35$ eV. Hence our experimental values agree remarkably well with theoretical predictions.

VIII. COMPARISON WITH PREVIOUS RESULTS

A. Dreybrodt *et al.* (1972)

The resonant Raman scattering (RRS) curves measured by Dreybrodt *et al.*[5] were fitted with expressions similar to Eq. (4). The function $d\chi/dE_1$ was replaced by $-d\chi/dE$, which is a good approximation near the crititcal-point energy. The derivative $d\chi/dE$ was taken from the experimental data of Shaklee *et al.*[20] For the three-band terms, one needs the function $\chi^+-\chi^-$. Dreybrodt *et al.*[5] assume

$$\chi^+(E)\approx\chi(E),\quad \chi^-(E)\approx 0 \quad \text{for } E\sim E_1\ . \tag{14}$$

This is a good approximation for the imaginary part of the χ's because the spin-orbit splitting is much larger than the broadening of the critical points under consideration. The approximation is not as good for the real parts; however, possible differences can be absorbed in the real constant C added to the Raman polarizability by these authors. The function $\chi(E)$ was obtained by integration of the derivative spectrum of Shaklee *et al.* This integration gives χ values which are 60% higher than those obtained here.

As a fitting parameter, the ratio $d^5_{3,0}/d^5_{1,0}=-2$ was determined. However, Dreybrodt *et al.* used a different definition of $d^5_{3,0}$ [compare their Eq. (1) with our Eq. (4)]. In the notation of this work, their result would read $d^5_{3,0}/d^5_{1,0}=-1.2$. The difference between both results arises mainly from the different values used for the function $\chi^+-\chi^-$.

B. Dreybrodt *et al.* (1973)

The experimental results of Dreybrodt[6] (1973) are essentially the same as those of Ref. 5. The two- and three-band coefficients, however, cannot be directly compared with the other determinations (Refs. 5 and 7, this work) because there is an error in Eq. (3) of Ref. 6, leading to different units for the interaction coefficients.

C. Richter *et al.* (1978)

For the two-band terms, these authors[7] used[26] the experimental $d\chi/dE$ of Shaklee *et al.*[20] as in Ref. 5, but for the three-band terms they performed a numerical calculation of $\chi^+-\chi^-$ from $\chi(\omega)$ of Ref. 27. They calculated that $\mathrm{Im}(\chi^+-\chi^-)$ has a maximum value of 1, while our measured $\mathrm{Im}\chi$ has a maximum of about 1.5. This difference is too large, since, in view of the approximate validity of Eq. (14), as discussed above, these two values should be very similar. The ratio $d^5_{3,0}/d^5_{1,0}$ was found to be -7. The difference with Ref. 5 can be traced back to the different values attributed to the function $\chi^+-\chi^-$ and to the fact that Richter *et al.* not only fitted the resonance shape, but also the enhancement under uniaxial stress. The result $d^5_{3,0}/d^5_{1,0}=-7$, however, is also different from our $d^5_{3,0}/d^5_{1,0}=-2$. This is again due to differences between the values for $\mathrm{Im}(\chi^+-\chi^-)$ in both works and to the fact that the imaginary part of $d\chi/dE$ is enhanced in Ref. 7 with respect to our ellipsometric results.

Opposite signs of $d^5_{3,0}$ and $d^5_{1,0}$ were found to be necessary to explain the antiresonance in the TO-RRS spectra above E_1.[5,7] The explanation given in Refs. 5 and 7 is that for $d^5_{3,0}/d^5_{1,0}<0$, the two- and three-band terms interfere destructively above the gap. Although there are indications of this antiresonance in our experimental spectra [Fig. 2(a)], we have not been able to obtain any antiresonance above E_1 in the theoretical curve, neither with the original data of Shaklee nor with our new ellipsometric results for χ. However, we also find that $d^5_{3,0}/d^5_{1,0}$ must be negative. Otherwise, two- and three-band terms tend to interfere destructively at the gap energy. In particular, we do not find any resonance enhancement under uniaxial stress with $d^5_{3,0}/d^5_{1,0}>0$.

The dominance of two-band terms in InSb was attributed to the larger spin-orbit splitting in InSb compared with Ge (where the resonance can be explained to a good approximation with three-band terms only[3,14]). It is clear from Eq. (4) that the larger the spin-orbit splitting Δ_1, the smaller the three-band contribution becomes. A second

reason for the difference between Ge and InSb was found in the stronger excitonic effects in InSb. According to Richter *et al.*, the derivative $d\chi/d\omega$ is six times larger in InSb due to excitonic effects. This last statement is wrong. The factor is actually not 6, but merely a number between 1 and 2. This can also be clearly seen by comparing the second derivatives of χ both materials.[12,13]

ACKNOWLEDGMENTS

This work was made possible by the help of W. Richter, who kindly provided us with his old data files, programs, and figures. Thanks are also due to P. Wurster, H. Hirt, and M. Siemers for technical assistance.

*Present address: IBM Thomas J. Watson Research Center, Yorktown Heights, NY 10598.

†On leave from Physics Laboratory III, National Technical University, Zografou Campus, Athens 624, Greece.

[1]A. Pinczuk and E. Burstein, Phys. Rev. Lett. **21**, 1073 (1968).

[2]R. C. C. Leite and J. F. Scott, Phys. Rev. Lett. **22**, 130 (1969).

[3]F. Cerdeira, W. Dreybrodt, and M. Cardona, Solid State Commun. **10**, 591 (1972).

[4]P. Y. Yu and Y. R. Shen, Phys. Rev. Lett. **29**, 468 (1972).

[5]W. Dreybrodt, W. Richter, and M. Cardona, Solid State Commun. **11**, 1127 (1972).

[6]W. Dreybrodt, W. Richter, F. Cerdeira, and M. Cardona, Phys. Status Solidi B **60**, 145 (1973).

[7]W. Richter, R. Zeyher, and M. Cardona, Phys. Rev. B **18**, 4312 (1978).

[8]See, for example, P. Vogl, in *Physics of Nonlinear Transport in Semiconductors,* edited by D. K. Ferry, J. R. Barker, and C. Jacoboni (Plenum, New York, 1980).

[9]W. Richter, in *Solid State Physics,* Vol. 78 of *Springer Tracts in Modern Physics,* edited by G. Höhler (Springer, Berlin, 1976), p. 121.

[10]M. Cardona, in *Light Scattering in Solids II,* Vol. 50 of *Topics in Applied Physics,* edited by M. Cardona and G. Güntherodt (Springer, Berlin, 1982), p. 19.

[11]J. Menéndez and M. Cardona, Phys. Rev. Lett. **51**, 1297 (1983); Phys. Rev. B **31**, 3696 (1985).

[12]L. Viña, S. Logothetidis, and M. Cardona, Phys. Rev. B **30**, 1979 (1984).

[13]S. Logothetidis, L. Viña, and M. Cardona, Phys. Rev. B **31**, 947 (1985).

[14]A. K. Sood, G. Contreras, and M. Cardona, Phys. Rev. B **31**, 3760 (1985).

[15]A. A. Gogolin and E. I. Rashba, Solid State Commun. **19**, 1177 (1976).

[16]W. Bauhofer (private communication).

[17]J. Wagner and M. Cardona, Solid State Commun. **48**, 301 (1983).

[18]W. C. Dash and R. Newman, Phys. Rev. **99**, 1151 (1955).

[19]D. E. Aspnes and A. A. Studna, Phys. Rev. B **27**, 985 (1983).

[20]K. L. Shaklee, J. E. Rowe, and M. Cardona, Phys. Rev. **174**, 828 (1968); see also K. L. Shaklee, Ph.D. thesis, Brown University, 1969.

[21]H. J. Mattausch and D. E. Aspnes, Phys. Rev. B **23**, 1896 (1981).

[22]W. Pötz and P. Vogl, Phys. Rev. B **24**, 2025 (1981).

[23]J. Menéndez, M. Cardona, and L. K. Vodopyanov, Phys. Rev. B **31**, 3705 (1985).

[24]R. M. Martin, Phys. Rev. B **10**, 2620 (1974).

[25]H. Presting (private communication).

[26]W. Richter (private communication).

[27]H. Philipp and H. Ehrenreich, Phys. Rev. **185**, 1103 (1969).